# Tunable Acoustic Nonreciprocity in Strongly Nonlinear Waveguides with Asymmetry

Alireza Mojahed,[*] Jonathan Bunyan,[†] Sameh Tawfick,[‡] and Alexander F. Vakakis[§]
*Department of Mechanical Science and Engineering, University of Illinois, Urbana, Illinois 61801, USA*

(Received 2 April 2019; revised manuscript received 3 June 2019; published 17 September 2019; corrected 10 July 2020)

In linear acoustics, the reciprocal behavior of waves traveling in periodic materials can be manipulated by imposing external or configurational biases to the system. However, the nonreciprocity observed in linear systems is energetically expensive. We demonstrate that strongly nonlinear, asymmetric lattices can be designed to exhibit strong nonreciprocity that is passively adaptive and tunable. An alternative class of waveguides consisting of two coupled nonlinear lattices, one stiffer than the other, allows wave propagation preferentially in one direction at certain energy ranges. This "giant" nonreciprocal behavior is obtained passively by tuning the propagation zones of these lattices in the frequency-energy domain. We present numerical simulations corroborated by experiments to show an instance of this alternative class of nonlinear waveguides. Specifically, at low input energy, wave packets generated by an applied impulse at the lateral boundaries of the waveguide are blocked at the interface of the two lattices. However, at intermediate energy ranges, wave packets initiated at the free boundary of the softer lattice propagate through the waveguide, whereas wave packets initiated at the free boundary of the stiffer lattice are blocked at the interface. The nonreciprocal acoustics persist until at the critical level of input energy, above which waves propagate in both directions within the waveguide. The range of energy over which nonreciprocal wave transmission occurs is passively tunable by appropriately manipulating the nonlinear propagation zones of the lattices in the frequency-energy domain. The nonreciprocity concept is applicable to materials and systems capable of exhibiting strongly nonlinear behavior and can find broad applications in cases where passive targeted (directed) energy transfer in space and/or frequency is a desired outcome. For example, nonlinear nonreciprocal metamaterials can be used in passive acoustic isolation designs with the capacity for unidirectional sound transmission, thus eliminating their "acoustic signature"; in ultrasonics, to yield better wave focusing at preferential frequencies, and thus improved signal-to-noise ratios; in shock isolation systems, for example, by rapid nonreciprocal low-to-high nonlinear energy transfers, yielding fast structural response attenuation; or in networks of coupled oscillators enabling passive, irreversible energy transmission in preferential directions. Clearly, such capabilities for passive nonreciprocity are not attainable in linear systems.

DOI: 10.1103/PhysRevApplied.12.034033

## I. INTRODUCTION

Reciprocity is a fundamental property of linear time invariant (LTI) systems that are governed by self-adjoint operators and is a consequence of their symmetric Green's functions [1]. Reciprocity is directly related to time-reversal symmetry through the Onsager-Casimir principle of microscopic reversibility [2–4], so reciprocity breaking is only possible by breaking the time-reversal symmetry on the microlevel [5]. Recently, this area has attracted considerable interest due to its important potential applications, for example, mechanical diodes, acoustic logic, and targeted (irreversible) wave, sound, and energy transmission. Common approaches to break reciprocity (and time-reversal symmetry) in LTI systems include applying odd-symmetric external biases [6–8] or by inducing time-variant properties [7,9,10]. Indeed, Popa and Cummer achieved wave isolation factors over 10 dB by coupling an active metamaterial to a nonlinear electronic circuit [9]. In that system, all three cited approaches were employed to break the Onsager-Casimir principle of microscopic reversibility. Another example of biased wave propagation are sytems whose physical properties are spatiotemporally modulated, such as acoustic circulators [11], graphene-based nanoelectromechanical systems (NEMS) [6], and various types of electromechanical systems [12–15]. While these approaches are attractive, the introduction of external biases or time-varying properties requires an external energy source (making these designs nonpassive) and are

[*]mojahed2@illinois.edu
[†]jbunyan2@illinois.edu
[‡]tawfick@illinois.edu
[§]avakakis@illinois.edu

 © 2019 American Physical Society

less effective under broadband impulse excitations. An alternative approach recently explored is through utilizing intentional nonlinearities, yielding completely passive nonreciprocity without the need for external energy input or external biases. Moreover, it has been shown that nonlinearity in itself, although necessary, is not sufficient for passive breaking of reciprocity, since several additional factors are important, including the boundary conditions, the asymmetries of the governing nonlinear operators, and the choice of the spatial points where the nonreciprocity criterion is tested [16]. For example, lattice materials incorporating nonlinear stiffness elements, asymmetry, and scale hierarchy exhibit nonreciprocity under impulse excitation [17] as they support nonlinear targeted (irreversible) energy transfers across spatial and/or temporal scales. As shown in [17], the governing nonlinear mechanism for nonlinear reciprocity breaking is transient resonance capture [18], a concept that can be effectively translated to designing nonreciprocal cellular lattice materials.

In this study, we consider a nonlinear, asymmetric lattice waveguide that passively breaks acoustic reciprocity without requiring any external biases or any other source of energy. Considering one-dimensional wave transmission, we study this waveguide using numerical simulations and validate our theoretical predictions experimentally. The waveguide entails a lattice material capable of transmitting acoustic waves in one direction, while arresting their propagation in the opposite direction. We accomplish this by coupling two dissimilar, strongly nonlinear lattices—in which the linear elastic components in the nonlinear stiffness elements are negligible. Each lattice has uniform dynamic properties throughout, however, compared to each other, they only defer in their elastic on-site stiffness, henceforth referred to as the "stiff" and "soft" lattices. The introduction of such intentional nonlinearities and asymmetries permits passive tunability of the system through strong frequency-energy dependence.

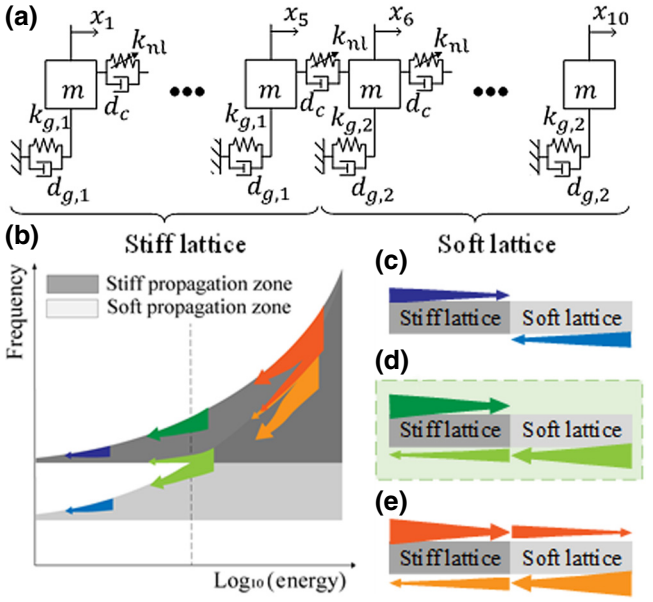


FIG. 1. Nonreciprocal 10-cell waveguide composed of two dissimilar lattices: (a) Reduced order model of the waveguide with uniform nonlinear coupling elements—the "stiff" lattice is composed of cells 1 to 5 with springs and viscous dampers $k_{g,1}$ and $d_{g,1}$, respectively, whereas the "soft" lattice consists of cells 6 to 10 with parameters $k_{g,2}$ and $d_{g,2}$. (b) Breather transmission in the propagation zones (PZs) of the two lattices, with the breather frequency band represented by arrows for weak (blue), critical (green), and strong (orange) impulsive excitation applied to the free end of the stiff (darker shade) or soft (lighter shade) lattice—forks in the arrows indicate successful initiation of a wave packet in the PZ of the downstream lattice. (c-e) Schematic representation of breather propagation in the waveguide for weak (c), critical (d), and strong (e) excitation, respectively—darker colored arrows denote stiff-soft, and lighter colored arrows soft-stiff direction of propagation.

## II. MODEL OF THE PROBLEM AND BACKGROUND CONCEPTS

A reduced order model (ROM) for the waveguide is depicted in Fig. 1(a). The waveguide consists of an array of 10 cells, with each cell consisting of a lumped mass $m$ that is grounded by a linear spring ($k_{g,1}$ or $k_{g,2}$)—viscous damper ($d_{g,1}$ or $d_{g,2}$) pair. All cells are coupled by means of uniform nonlinear stiffnesses ($k_{\rm nl}$)—viscous damping ($d_c$) pairs. If $k_{g,1} > k_{g,2}$, the left five cells comprise the "stiff" lattice, and the right five cells the "soft" lattice. Moreover, the force-displacement characteristic of each nonlinear coupling stiffness is assumed to be in the form $F = k_{\rm nl}\delta^3$ where $\delta$ is the extension of the nonlinear spring, $F$ is the resulting force, and the value of $k_{\rm nl}$ is constant along the waveguide; it follows that the waveguide is strongly nonlinear, since the coupling stiffnesses lack any linear components, although the results will not be affected by the presence of a small linear component. The inclusion of strong stiffness nonlinearity is an important requirement in our nonreciprocal approach as it is needed to initiate the governing transient resonance captures and targeted energy transfers that break reciprocity [17]. Hence, the nonlinear waveguide is the combination of a left stiff lattice and a right soft lattice. The left end of the stiff lattice and the right end of the soft lattice are free, and the nonlinear stiffness—viscous damper pair that couples the fifth cell (right-most cell of the stiff lattice) and the sixth cell (left-most of the soft lattice) is henceforth referred to as the "interface" or "interfacial coupling" of the two lattices. Considering one-dimensional acoustics and for a given direction of wave propagation, the lattices preceding and following the interface are referred to as the "upstream" and 'downstream' lattices, respectively. The acoustics of uniform and boundless analogs of these lattices were recently studied analytically and numerically

in [23], and it was found that they can support traveling breathers. These are traveling oscillatory wave packets with spatially localized envelopes that possess two distinct time scales, namely, a fast time scale governing the oscillations of the individual particles of the lattice during breather transmission, and a slow time scale governing the temporal evolution of the localized envelope that modulates the fast oscillations [19–22]. Moreover, as shown in [23], traveling breathers in the uniform, boundless nonlinear lattice are realized close to the upper boundary of its propagation zone (PZ) and depend on energy. Similar to linear periodic systems, a PZ is defined as the region in the frequency-energy plane where wave packets can propagate unhindered in the unbounded nonlinear uniform lattice; the complementary regions in the frequency-energy domain then define attenuation zones (AZs) where no traveling wave packets can be realized, and only localized near-field waves exist. In contrast to linear PZs, however, nonlinear PZs are energy dependent [23,24].

Considering the waveguide of Fig. 1(a), the infinite (boundless) extensions of the stiff and soft constituent lattices possess their own PZs at different frequency ranges and are dependent on energy [cf. Fig. 1(b)]. The asymmetry between the PZs of the stiff and soft lattices is key to breaking acoustic reciprocity in the nonlinear waveguide. The equations of motion of the 10-cell waveguide are given by

$$m\ddot{x}_i + d_{g,j}\dot{x}_i + k_{g,j}x_i + d_c(\dot{x}_i - \dot{x}_{i-1}) + k_{nl}(x_i - x_{i-1})^3 + d_c(\dot{x}_i - \dot{x}_{i+1}) + k_{nl}(x_i - x_{i+1})^3 = 0, \quad (1)$$

where $j = 1$ for $i = 1, \ldots, 5$ and $j = 2$ for $i = 6, \ldots, 10$. As discussed in [25], a method to approximate the PZs of the two lattices is to compute their nonlinear normal modes (NNMs) [26], that is, the periodic orbits of the detached lattices. Then the lowest (highest) in-phase mode (out-of-phase NNM) provides an approximation to the upper (lower) boundary of the PZ of the corresponding lattice. This is performed numerically using the program NNMcont [27]. The boundaries of the PZs of the two lattices are schematically represented in Fig. 1(b), where the offset and overlap between the PZs of the stiff and soft lattices can be tuned by adjusting the values of the linear grounding stiffnesses $k_{g,1}$ and $k_{g,2}$. Since the in-phase mode of each lattice does not involve deformations of the nonlinear coupling stiffnesses, it is linear and subsequently does not depend on energy; accordingly, the lower bound of each PZ is a horizontal line in the frequency-energy domain. In contrast, the out-of-phase mode is strongly nonlinear since it involves deformations of the nonlinear coupling stiffnesses, so the upper boundary of each PZ exhibits strong stiffening behavior with its frequency increasing with energy [cf. Fig. 1(b)].

## III. GOVERNING MECHANISM OF THE NONLINEAR ACOUSTIC NONRECIPROCITY

Considering each of the two lattices, a traveling wave packet (e.g., breather) can be initiated if it contains frequencies within the corresponding PZ. The unique feature, however, of the nonlinear waveguide is that the PZs of the two constituent lattices are tunable with energy. Accordingly, while the PZs of the soft and stiff lattices are separated at low energy levels (so they allow for propagation of wave packets only in one of the two lattices, but not through their interface), the PZs have partial overlap at higher energies [cf. Fig. 1(b)]. This indicates that traveling acoustic wave packets in the common area of the two PZs could potentially be transmitted through the interface between the soft and stiff lattices. Motivated by this observation, we design the overlap between the two PZs to occur at practical energy levels, indicated by the vertical dashed line in Fig. 1(b). The grounding linear stiffness coefficients, $k_{g,1}$ and $k_{g,2}$, and the other system parameters are listed in Table 1. These values correspond to the corresponding averaged parameter values that are identified for the experimental realization of the waveguide, as discussed below.

The mechanism governing nonlinear nonreciprocity in the waveguide is now described. We note at this point that we will focus only on the primary wave propagation, that is, only on the traveling breathers [23] initiated in either lattice following the application of impulses at one of the free boundaries of the waveguide. We will consider traveling breathers initiated by impulses applied to cell 1 (the first cell of the stiff lattice) and propagating toward the interface with the soft lattice—henceforth referred to [23] as the stiff-soft direction and represented schematically by the thicker colored arrows in Fig. 1(b). In the opposite soft-stiff direction, traveling breathers are initiated at cell 10 (the last cell of the soft lattice) and propagate toward the interface with the stiff lattice—these are represented by the lighter shaded arrows in Fig. 1(b). In both cases, the frequency contents of the propagating breathers lie just outside the upper boundaries of the corresponding PZs of the lattices where they are initiated [23] and follow these upper boundaries with decreasing energy due to viscous dissipation and/or residual local "ringing" at the sites of the individual oscillators of the waveguide after passing of the breathers. Given, however, that the PZs of the two lattices are highly tunable with energy, depending on the intensity of the applied impulse, we need to distinguish

TABLE I. System parameters for the waveguide.

| $m$ (kg) | $k_{g,1}$ (N/m) | $d_{g_1}$ (Ns/m) | $k_{g,2}$ (N/m) | $d_{g_2}$ (Ns/m) | $k_{\rm nl}$ (N/m$^3$) | $d_c$ (Ns/m) |
|---|---|---|---|---|---|---|
| 0.022 | 1467.27 | 0.085 | 687.53 | 0.11 | 2.48E9 | 0.0805 |

between three energy regimes, as schematically described in Figs. 1(b)–1(e).

For weak excitations (blue arrows in Fig. 1), traveling breathers can only propagate through the lattice where they are initiated due to the absence of overlap between the PZs of the stiff and soft lattices at low energies [cf. Figs. 1(b) and 1(c)]; as a result, incoming breathers are reflected at the interface from either direction. Critical-energy excitations (green arrows in Fig. 1) correspond to energies close to the energy level where the PZs of the two lattices start overlapping [cf. dashed line in Fig. 1(b)]. Hence, propagating breathers in the soft-stiff direction are partially transmitted through the interface, since their frequency content partially overlaps with the PZ of the stiff lattice, thus they can initiate traveling wave packets in the stiff lattice; this is schematically presented by the bifurcating "fork" of the light green arrow in Fig. 1(b). On the contrary, propagating breathers in the stiff-soft direction are reflected at the interface since their frequency content does not overlap with the PZ of the soft lattice, and thus cannot initiate traveling wave packets across the interface. This results in strong acoustic nonreciprocity ("giant" nonreciprocity) at that energy range [cf. Figs. 1(b) and 1(d)]. Finally, for strong excitations (orange arrows in Fig. 1), propagating wave packets initiated in both soft-stiff and stiff-soft directions have frequency contents that overlap with both PZs [cf. bifurcated forks in Fig. 1(b)] thus allowing for wave transmission through the interface in both directions. We note that since the location of the two PZs along the frequency axis depends on the grounding linear stiffness coefficients, $k_{g,1}$ and $k_{g,2}$, the excitation levels for the three previous acoustic regimes of the waveguide can be tuned by appropriate design.

## IV. RESULTS AND DISCUSSION

### A. Numerical study

To highlight acoustic nonreciprocity in the nonlinear waveguide, we perform a series of numerical simulations of the ROM (1) using a fourth-order Runge-Kutta scheme. Assuming zero initial conditions, the impulsive force recorded by the force transducer from the experiments is applied to the free boundaries of the ROM (1). Based on the derived numerical results, we compute the instantaneous total energies of the unit cells, and through interpolation in space and time, the spatio-temporal energy evolution in the entire waveguide, as shown in Figs. 2(a)–2(c). For clarity and to account for the diminishing wave amplitudes due to viscous dissipation, at each time instant, the energy of each cell is normalized with respect to the maximum instantaneous value of the total energy of the entire waveguide; hence, at each time instant, the plotted energy is normalized from zero to unity. Considering the results, following the application of the impulse, a traveling breather is initiated in the stiff or soft lattice and propagates toward the interface. Depending on the direction of wave propagation and the amplitude (energy) of the impulse, different wave scattering phenomena occur at the interface, as discussed previously.

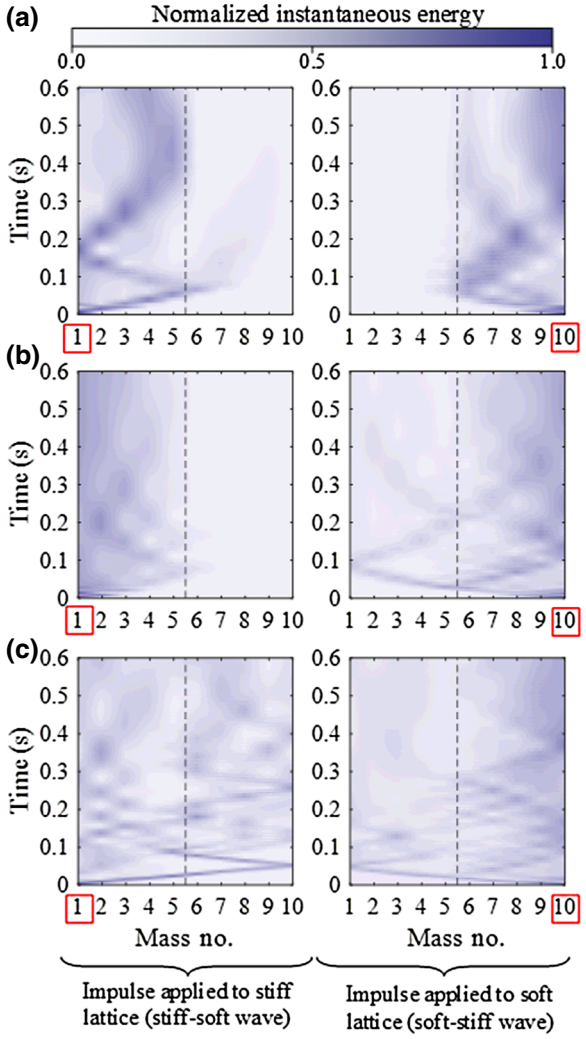


FIG. 2. Computational spatio-temporal evolution of the total instantaneous energy in the waveguide for an impulse applied to the stiff (left column) and soft (right column) lattice, with red squares indicating the cell where the impulsive force, measured from the experiments, is applied, and darker shades corresponding to higher energy levels. (a) Weak impulses—16.75 N impulse amplitude for the stiff and 15.64 N for the soft lattice. (b) Critical-energy impulses—31.96 N for the stiff and 31.47 N for the soft lattice. (c) Strong impulses—55.18 N for the stiff and 53.04 N for the soft lattice (for clarity and to account for viscous dissipation, at each time instant, the energy is normalized with respect to the maximum instantaneous energy at that time instant).

Focusing exclusively on primary wave propagation, for weak excitation, the breather propagates only in the lattice where it is initiated and is reflected at the interface [cf. Figs. 2(a) and 1(b)]. After reflection of the breather

at the interface, there occur secondary reflections but, again, these are localized in the lattice that is excited by the impulse. A different result is obtained, however, for critical-energy excitation, as shown in Fig. 2(b). In this case, the breather initiated in the soft lattice is only partially reflected at the interface, while a propagating wave packet is transmitted in the stiff lattice according to the schematic of Fig. 1(b). On the contrary, the breather initiated in the stiff lattice is completely reflected at the interface, again in accordance with the schematic of Fig. 1(b). This results in "giant" nonreciprocity in the waveguide, as waves can propagate in the soft-stiff direction but not in the stiff-soft direction. Finally, for strong excitation, cf. Fig. 2(c), traveling wave packets can transmit in both directions, undergoing only partial reflections at the interface, in agreement with our predictions in Fig. 1(b). We emphasize at this point that following the excitation of the primary wave packet (breather) by the applied impulse, additional interactions between the wave packet and its "tail," occur as well as secondary interfacial reflections, but they are at very low energy levels and are inconsequential to the overall acoustics. This justifies our focus on primary wave propagation. In our numerical study, the amplitudes of the impulse loads are chosen to be identical to the ones used in the experimental study described below. Based on our numerical study of the ROM (1), the regime of "giant" nonreciprocity (only soft-stiff wave transmission) is realized in the range of impulsive amplitudes 25.9 to 45 $N$. Below that range, there occurs complete breather reflection at the interface (regime of weak excitation) and above it, transmission of waves in both stiff-soft and soft-stiff directions (regime of strong excitations).

### B. Experimental validation

To corroborate the previous computational results, we perform a series of experimental measurements. Figures 3(a) and 3(b) depict the schematic and experimental realization of the experimental fixture corresponding to the 10–cell ROM of Fig. 1(a). Each unit cell is composed of an aluminum mass whose unidirectional motion is tracked through an attached accelerometer. The aluminum mass is grounded by a pair of 50 - $\mu$m-thick 1080 spring steel flexures, which, under bending, provide the linear grounding stiffness of the ROM. This stiffness is adjusted by cutting out square sections of the flexure to produce different force-extension relationships for the stiff and soft lattice groundings with stiffness constants $k_{g,1}$ and $k_{g,2}$, respectively [cf. Fig. 3(c)]. This method of stiffness tuning is robust and can be used to reliably produce a variety of stiffnesses to shift the PZs of the stiff and soft lattices as desired. Hence, we can experimentally tune the energy levels corresponding to the three previously discussed regimes of passive nonreciprocity. Neighboring unit cells are coupled to each other through clamped 0.006-in.-thick

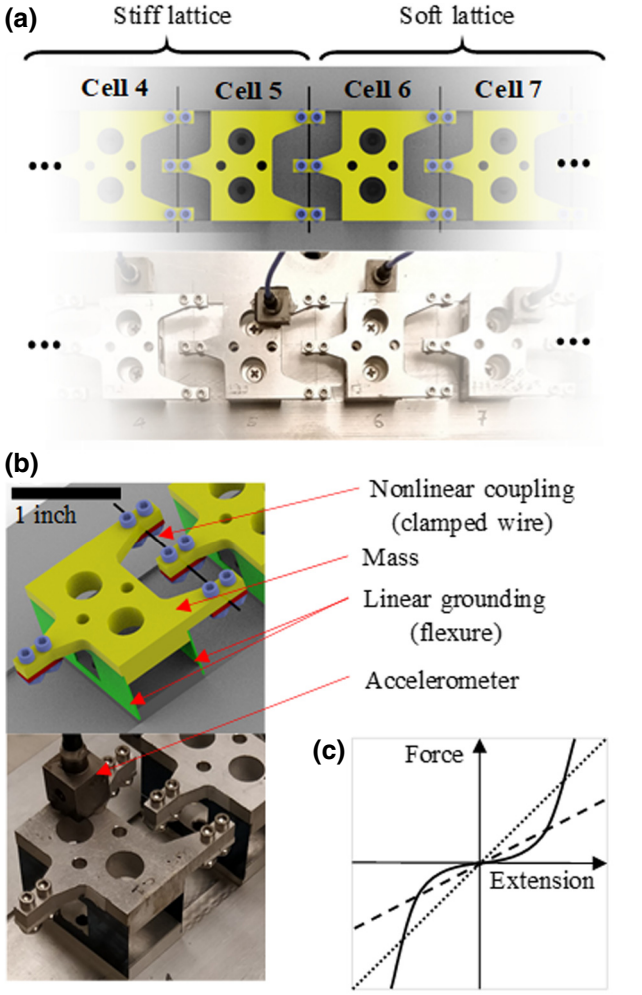


FIG. 3. Waveguide composed of 10 unit cells: (a) Schematic top view of unit cells 4-7 (top) and experimental realization (bottom); the waveguide is excited with a modal hammer fitted with a force transducer, and the response of each unit cell is measured by means of ten accelerometers attached to the cells. (b) Detailed isometric view of the schematic design and the experimental realization of the first unit cell showing the aluminum mass (yellow) grounded to a rigid frame (gray) through linear flexure springs (green) whose stiffness is tuned through the geometry of the flexures; adjacent unit cells are coupled through thin wires (black) attached by clamps (red) and bolts (purple) —this provides the essentially nonlinear stiffness. (c) Schematic representation of the force-extension relationships of the different stiffness elements of the waveguide—stiff linear grounding $k_{g,1}$ (dotted line), soft linear grounding $k_{g,2}$ (dashed line), and nonlinear coupling $k_{\mathrm{nl}}$ (solid line), which are responsible for the frequency-energy tunability of the two PZs of the constituent lattices of the waveguide.

1080 spring steel clamped wires, with special care being taken to maintain each wire in a nearly untensioned and/or unbuckled state during assembly. Ideally, each untensioned clamped wire under transverse deformation at its center acts as an essentially nonlinear cubic spring, that is, it possesses a cubic nonlinear force-extension relationship

with no linear component [cf. schematic representation in Fig. 3(c)] [28,29]. However, in practice, due to their thickness, the wires always possess a small bending stiffness, so they behave like thin Euler-Bernoulli beams at very small deflections. This gives rise to a small linear stiffness in addition to the strongly nonlinear cubic stiffness, but this does not affect the nonreciprocity results. It follows that a small linear term in this coupling spring is unavoidable in practice, but this can be made small by reducing the thickness-to-length ratio of the clamped wires as much as possible (see Supplemental Material [30]).

The waveguide is excited by a modal hammer with a force transducer attached to its impacting head to experimentally measure the applied impulsive force. Data is collected from both this force transducer and the 10 accelerometers attached to the unit cells through an m + p VibPilot dynamic system analyzer. Due to the inherent variation in manufacturing, tolerances, and other unmodeled effects, the masses, stiffnesses, and structural damping coefficients of the 10 cells of the experimental waveguide cannot be identical (as in the theoretical ROM). Furthermore, since the excitation is provided manually through the modal hammer, exact replication of the impulsive loads in the soft-stiff and stiff-soft directions is not possible experimentally. The mass of each unit cell (including adjustments for the attached accelerometer) is measured, and their linear and nonlinear stiffnesses, as well as the damping coefficients in the grounding flexures and the coupling elements are estimated through nonlinear system identification [31–34] following the restoring-force method adapted from [17, 24]. The average values of the identified parameters are listed in Table 1 (see Supplemental Material [30]).

The experimental spatio-temporal energy plots to verify the previous three theoretical nonreciprocity regimes (cf. Fig. 2) are then constructed as follows. Following the application of the impulsive load, acceleration measurements for the unit cells are postprocessed (filtered, detrended, and numerically integrated) to estimate the cell displacements. Several tests are conducted at various excitation levels in both the stiff-soft and soft-stiff directions and the processed data is used in conjunction with the parameters from the system identification to compute the instantaneous total energy of each unit cell as a function of time. We then compute spatio-temporal energy plots at weak, critical, and strong energy levels in both directions as depicted in Figs. 4(a)–4(c). These plots represent the experimentally realized counterparts of the computational results of Figs. 2(a)–2(c). Focusing on primary wave propagation, the case of weak impulsive excitation is considered in Fig. 4(a). Similar to the theoretical prediction, the primary breathers that are initiated by the applied impulse only propagate in the upstream lattices and are completely reflected at the interface. In the case of critical energy excitation [cf. Fig. 4(b)] there is complete wave propagation

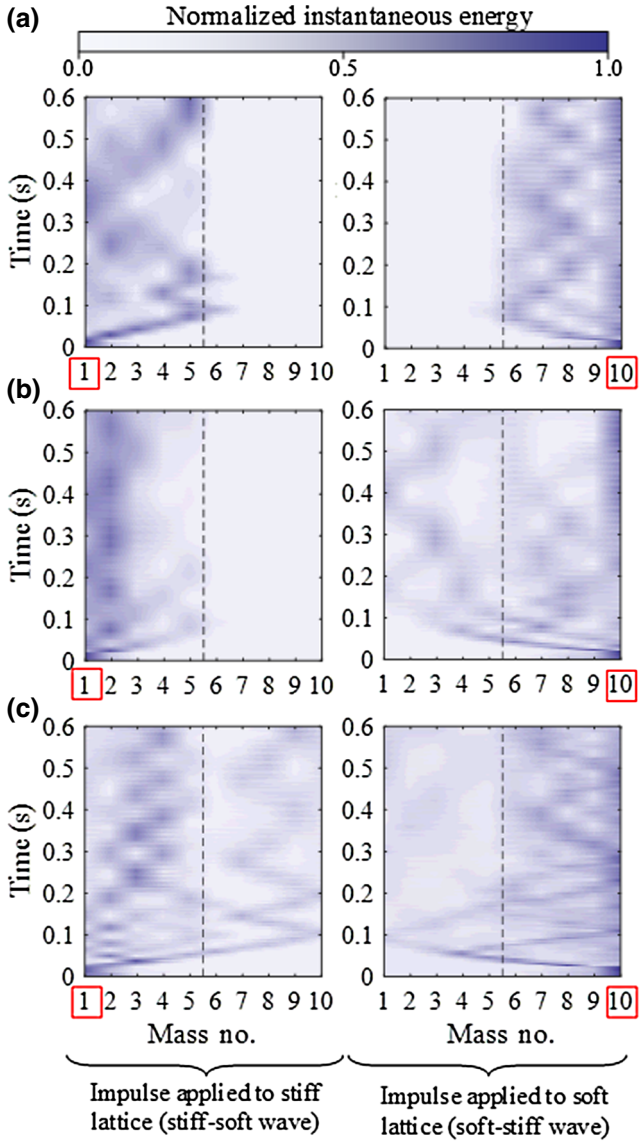


FIG. 4. Experimental spatio-temporal evolution of the total instantaneous energy in the waveguide for an impulse applied to the stiff (left column) and soft (right column) lattices, with red squares indicating the cell where the impulse is applied, and darker shades corresponding to higher energy levels. (a) Weak impulses, (b) critical-energy impulses, and (c) strong impulses—in all cases the impulse magnitudes are identical to those of the numerical simulations of Fig. 2 (for clarity and to account for viscous dissipation, at each time instant, the energy of each cell is normalized with respect to the maximum instantaneous energy of the waveguide at that time instant).

in the soft-stiff direction but not in the stiff-soft direction, again confirming the theoretical findings. Finally, in the case of strong excitation [cf. Fig. 4(c)] as predicted, there is wave transmission and partial reflection at the interface in both directions. Hence, the three computational nonlinear nonreciprocity regimes are reproduced in the experiments. The experimental regime of "giant" nonreciprocity (only

soft-stiff wave transmission) is found in the approximate range of impulsive amplitudes 25.9 to 49 $N$, and below or above that range there occurs either a complete breather reflection at the interface or wave transmission in both stiff-soft and soft-stiff directions, respectively. The upper boundary of the experimental range slightly exceeds the corresponding computational value of 45 $N$. Following the primary wave, the simulation and experimental results for the secondary waves (generated by later reflections from the ends and/or the interface of the waveguide) agree to a lesser extent. These discrepancies are reasonable since the ROM (1) of the waveguide assumes uniformity in the stiff and soft constituent lattices and does not account for the slight parameter variations of the experimental waveguide nor for additional unmodeled experimental effects, for example, nonlinear friction, flexibility of the grounding flexures, or nonideal connections to ground and between cells.

To experimentally confirm the mechanism of nonlinear nonreciprocity of Fig. 1(b), we study the frequency content of the velocity responses of selected unit cells of the waveguide. This is achieved by computing wavelet transforms of the measured time series of the cells, depicting the temporal evolutions of the dominant harmonics of the corresponding responses. Specifically, we consider the responses of one cell upstream and two cells downstream of the interface. In the stiff-soft direction, we consider the responses of unit cells 5, 6, and 7, whereas in the soft-stiff direction, we considered the responses of cells 6, 5, and 4. The resulting wavelet transform spectra of the experimental responses shown in Figs. 4(a)–4(c) are depicted in Figs. 5(a)–5(c), respectively. The lower boundaries of the PZs of the stiff and soft lattices are represented in these plots as dark gray and light gray dashed horizontal lines, respectively. Moreover, the red triangles indicate the dominant frequency contents of the primary breather in the upstream lattice (following the application of the impulsive load) and the downstream transmitted wave packets; given that primary breather lies just above the upper boundary of the PZ of the upstream lattice, the red triangle in that case is consistent with the approximate location of this upper boundary at the corresponding energy level.

First, we consider the case of weak excitation depicted in Fig. 5(a). In the stiff-soft direction (see left plots) the incident breather has a frequency content just above the PZ of the upstream stiff lattice (see cell 5), and there are no frequency components in the PZ of the soft lattice (just above the gray dashed line) that are sufficiently strong to initiate a transmitted traveling wave packet in the downstream soft lattice (see cells 6 and 7). Likewise, in the soft-stiff direction (see right plots) there are no frequency components in the PZ of the downstream stiff lattice (see cells 4 and 5) indicating the absence of wave transmission through the interface of the two lattices. Different acoustic scattering phenomena occur in the case of the

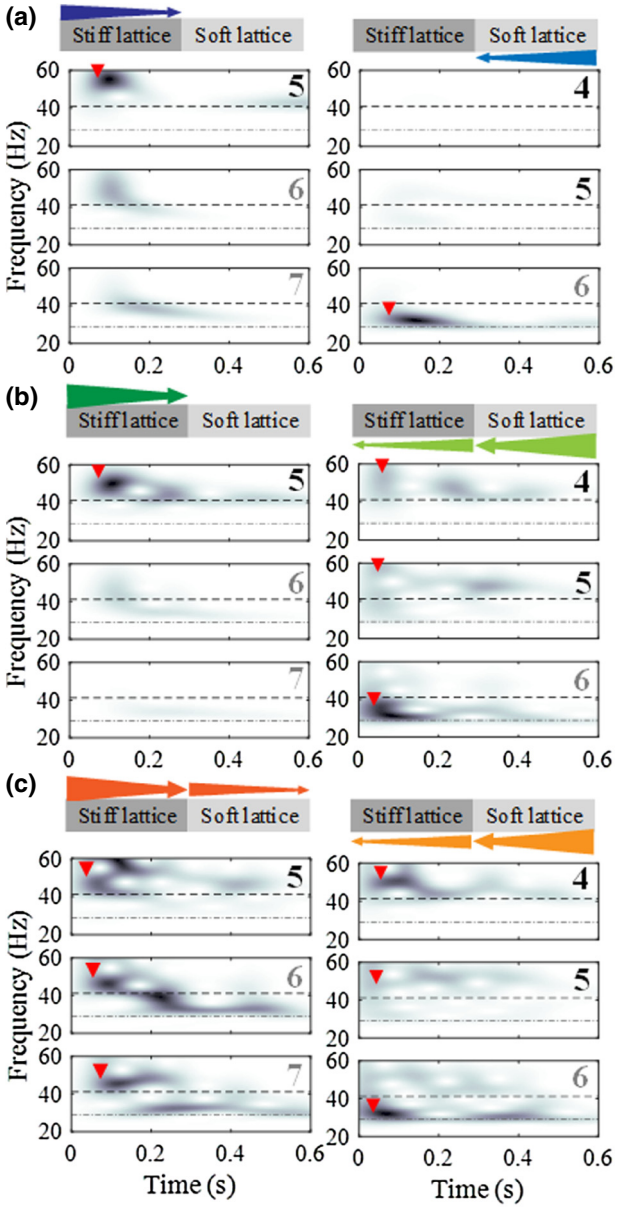


FIG. 5. Transient frequency content of the experimentally obtained velocities, one upstream and two downstream cells relative to the interface—cells 5-6-7 in the case of stiff-soft and cells 6-5-4 in the case of soft-stiff. Cell numbers are on the top right corner of each plot. Horizontal lines indicate the lower boundaries of the PZ of the stiff (black dashed) and soft (gray dash-dotted) lattices. Darker regions on the color map indicate a larger amplitude. Red triangles point to the frequency content in the primary wave as it propagates through each cell. (a) weak excitations of 16.75 N and 15.64 N applied to the stiff and soft lattices, respectively. (b) Critical excitations of 31.96 N and 31.47 N applied to the stiff and soft lattices, respectively. (c) Strong excitations of 55.18 N and 53.04 N applied to the stiff and soft lattices, respectively.

critical excitation considered in Fig. 5(b). Indeed, in the stiff-soft direction (see left plots) the incident primary breather has strong frequency content in the PZ of the

stiff lattice (see cell 5), but fails to transmit through the interface, as evidenced by the absence of strong frequency components in the PZ of the downstream soft lattice (see cells 6 and 7). However, a different picture is observed in the soft-stiff direction (see right plots) where the strong frequency content of the incident primary breather in the PZ of the soft lattice (see cell 6) "converts up" in frequency as the breather scatters at the interface, yielding strong frequency components in the PZ of the stiff lattice (see cells 5 and 4), thus initiating traveling wave packets downstream and across the interface. This results in acoustic nonreciprocity, confirming the theoretical scenario outlined in Fig. 1(b). Similar nonlinear scattering phenomena are observed for the case of strong impulsive excitation depicted in Fig. 5(c), where for both stiff-soft and soft-stiff directions there are "frequency-down" and "frequency-up" conversions, respectively, of the primary breathers in the upstream lattices, which enables their partial transmission through the interface to the corresponding downstream lattices. Hence, the theoretical predictions are fully confirmed by the experimental results.

## V. CONCLUSIONS

In synopsis, acoustic nonreciprocity in the considered waveguides is due to nonlinearity and asymmetry. The essentially nonlinear coupling stiffnesses plays two critical roles: They determine the shape of the upper bound of the PZs of the constituent lattices, which, unlike linear lattices, depend on energy, and they enable the initiation of traveling breathers in the upstream lattices, which provide the mechanisms for transferring energy in the spatio-temporal domain. The asymmetry is also important as it is responsible for frequency conversions during scattering of the incident primary breathers at the interface, which may enable partial wave transmission in the downstream lattice at certain energy ranges. We emphasize that the achieved break of acoustic reciprocity is completely passive, without requiring any external bias or energy source. Moreover, the waveguide can be tuned predictably to break reciprocity at different energy levels through the manipulation of the topologies of the PZs of the constituent lattices. Hence, the considered acoustic waveguide promotes an alternative passive scheme for achieving acoustic nonreciprocity without the need for external energy sources and time varying properties. Essentially, nonlinear lattices have already been shown to demonstrate useful properties such as energy-dependent acoustic filtering properties, nonreciprocal breather formation, and energy localization [35,36]. The acoustic nonreciprocity demonstrated in the asymmetric nonlinear lattices discussed in this work can find potential application in passive systems with inherent capacity for nonlinear targeted (directed) energy transfer in space and/or frequency. For example, nonreciprocal metamaterials supporting unidirectional sound transmission could be realized for unprecedented acoustic isolation. A different variant concerns protective metamaterial "shields" with the capacity for inherent energy scattering of incoming high-rate excitations (e.g., blasts) within the material through rapid low-to-high frequency and/or wave number nonlinear energy transfer for effective response reduction. Or, based on passive nonreciprocity, "nonlinear energy sinks" could be considered with enhanced capacity to absorb and harvest or locally dissipate broadband energy. Finally, the tunable (with energy) acoustic filtering properties of this type of nonreciprocal metamaterials could be used in better focusing and/or reduced scattering of ultrasonic waves to yield enhanced signal-to-noise ratios, or in designing networks of nonlinear oscillators with the capacity for directed energy transmission in preferential spatial directions. Clearly, no such effects can be induced in linear, time-invariant (LTI) systems.

## ACKNOWLEDGMENT

This work was supported in part by the National Science Foundation under NSF EFRI Grant No. 1741565.

[1] R. Courant and D. Hilbert, *Methods of mathematical physics [Methoden der mathematischen Physik, engl.] 1* (CUP Archive, New York and London, 1965).
[2] H. B. G. Casimir, On Onsager's principle of microscopic reversibility, Rev. Mod. Phys. **17**, 343 (1945).
[3] L. Onsager, Reciprocal relations in irreversible processes. I, Phys. Rev. **37**, 405 (1931).
[4] L. Onsager, Reciprocal relations in irreversible processes. II, Phys. Rev. **38**, 2265 (1931).
[5] R. Fleury, D. Sounas, M. R. Haberman, and A. Alù, Nonreciprocal acoustics, Acoust. Today **11**, 14 (2015).
[6] R. Fleury, D. L. Sounas, C. F. Sieck, M. R. Haberman, and A. Alù, Sound isolation and giant linear nonreciprocity in a compact acoustic circulator, Science **343**, 516 (2014).
[7] S. A. Cummer, Selecting the direction of sound transmission, Science **343**, 495 (2014).
[8] K. Tsakmakidis, L. Shen, S. Schulz, X. Zheng, J. Upham, X. Deng, H. Altug, A. Vakakis, and R. Boyd, Breaking Lorentz reciprocity to overcome the time-bandwidth limit in physics and engineering, Science **356**, 1260 (2017).
[9] B.-I. Popa and S. A. Cummer, Non-reciprocal and highly nonlinear active acoustic metamaterials, Nat. Commun. **5**, 3398 (2014).
[10] R. Fleury, D. L. Sounas, and A. Alù, Subwavelength ultrasonic circulator based on spatiotemporal modulation, Phys. Rev. B **91**, 174306 (2015).
[11] M. B. Zanjani, A. R. Davoyan, N. Engheta, and J. R. Lukes, NEMS with broken T symmetry: Graphene based unidirectional acoustic transmission lines, Sci. Rep. **5**, 9926 (2015).
[12] G. Trainiti and M. Ruzzene, Non-reciprocal elastic wave propagation in spatiotemporal periodic structures, New J. Phys. **18**, 083047 (2016).

[13] D.-W. Wang, H.-T. Zhou, M.-J. Guo, J.-X. Zhang, J. Evers, and S.-Y. Zhu, Optical Diode Made from a Moving Photonic Crystal, Phys. Rev. Lett. **110**, 093901 (2013).
[14] M. B. Zanjani, A. R. Davoyan, A. M. Mahmoud, N. Engheta, and J. R. Lukes, One-way phonon isolation in acoustic waveguides, Appl. Phys. Lett. **104**, 081905 (2014).
[15] J. C. Slater, Interaction of waves in crystals, Rev. Mod. Phys. **30**, 197 (1958).
[16] A. Blanchard, T. P. Sapsis, and A. F. Vakakis, Nonreciprocity in nonlinear elastodynamics, J. Sound Vib. **412**, 326 (2018).
[17] K. J. Moore, J. Bunyan, S. Tawfick, O. V. Gendelman, S. Li, M. Leamy, and A. F. Vakakis, Nonreciprocity in the dynamics of coupled oscillators with nonlinearity, asymmetry, and scale hierarchy, Phys. Rev. E **97**, 012219 (2018).
[18] J. P. Mücket, VI ARNOLD (Ed.): Dynamical systems III. Encyclopedia of mathematical sciences Vol. 3. Springer-Verlag, Berlin, Heidelberg, New York, London, Paris, Tokyo. 81 Abbildungen, XIV + 294 Seiten, Preis: DM 128,—. ISBN 0-387-17002-2 (V. 3), Astronomische Nachr. **310**, 379 (1989).
[19] S. Flach and K. Kladko, Moving discrete breathers?, Phys. D **127**, 61 (1999).
[20] S. Aubry and T. Cretegny, Mobility and reactivity of discrete breathers, Phys. D **119**, 34 (1998).
[21] R. MacKay, Discrete breathers: Classical and quantum, Phys. A **288**, 174 (2000).
[22] R. S. MacKay and J.-A. Sepulchre, Effective Hamiltonian for travelling discrete breathers, J. Phys. A: Math. Gen. **35**, 3985 (2002).
[23] A. Mojahed and A. F. Vakakis, Certain aspects of the acoustics of a strongly nonlinear discrete lattice, Nonlinear Dynamics (2019).
[24] J. Bunyan, K. J. Moore, A. Mojahed, M. D. Fronk, M. Leamy, S. Tawfick, and A. F. Vakakis, Acoustic nonreciprocity in a lattice incorporating nonlinearity, asymmetry, and internal scale hierarchy: Experimental study, Phys. Rev. E **97**, 052211 (2018).
[25] A. Mojahed, O. V. Gendelman, and A. F. Vakakis, Breather arrest, localization and acoustic non-reciprocity in dissipative nonlinear lattices, J. Acoust. Soc. Am. **146**, 826 (2019).
[26] A. Vakakis, L. Manevitch, Y. V. Mikhlin, V. Pilipchuk, and A. Zevin, *Normal Modes and Localization in Nonlinear Systems* (John Wiley & Sons, Inc, New York, 1996).
[27] M. Peeters, R. Viguié, G. Sérandour, G. Kerschen, and J. C. Golinval, Nonlinear normal modes, Part II: Toward a practical computation using numerical continuation techniques, Mech. Syst. Signal Process. **23**, 195 (2009).
[28] D. M. McFarland, L. A. Bergman, and A. F. Vakakis, Experimental study of non-linear energy pumping occurring at a single fast frequency, Int. J. Nonlin. Mech. **40**, 891 (2005).
[29] H. Cho, M.-F. Yu, A. F. Vakakis, L. A. Bergman, and D. M. McFarland, Tunable, broadband nonlinear nanomechanical resonator, Nano Lett. **10**, 1793 (2010).
[30] See Supplemental Material at http://link.aps.org/supplemental/10.1103/PhysRevApplied.12.034033 for the table of the identified parameters of the waveguide, a detailed discussion on the effects of inhomogeneity, and more details on the effects of linear stiffness component on the pass-bands structures.
[31] S. Masri and T. Caughey, A nonparametric identification technique for nonlinear dynamic problems, J. Appl. Mech. **46**, 433 (1979).
[32] G. Kerschen, V. Lenaerts, and J.-C. Golinval, VTT benchmark: Application of the restoring force surface method, Mech. Syst. Signal Process. **17**, 189 (2003).
[33] G. Kerschen, K. Worden, A. F. Vakakis, and J.-C. Golinval, Past, present and future of nonlinear system identification in structural dynamics, Mech. Syst. Signal Process. **20**, 505 (2006).
[34] J.-P. Noël and G. Kerschen, Nonlinear system identification in structural dynamics: 10 more years of progress, Mech. Syst. Signal Process. **83**, 2 (2017).
[35] M. A. Hasan, S. Cho, K. Remick, A. F. Vakakis, D. M. McFarland, and W. M. Kriven, Experimental study of nonlinear acoustic bands and propagating breathers in ordered granular media embedded in matrix, Granular Matter **17**, 49 (2015).
[36] K. Jayaprakash, Y. Starosvetsky, A. F. Vakakis, M. Peeters, and G. Kerschen, Nonlinear normal modes and band zones in granular chains with no pre-compression, Nonlinear Dynamics **63**, 359 (2011).

*Correction:* Equation (1) contained an error and has been fixed.